

Reaction Mechanisms

On the Mechanism of Bifunctional Squaramide-Catalyzed Organocatalytic Michael Addition; Protonated Catalyst as an Oxyanion Hole

Bianka Kótai,^[a] György Kardos,^[a] Andrea Hamza,^[a] Viktor Farkas,^[b] Imre Pápai,^{*[a]} and Tibor Soós^{*[a]}

Abstract: A joint experimental–theoretical study of a bifunctional squaramide-amine-catalyzed Michael addition reaction between 1,3-dioxo nucleophiles and nitrostyrene has been undertaken to gain insight into the nature of bifunctional organocatalytic activation. For this highly stereoselective reaction, three previously proposed mechanistic scenarios for the critical C–C bond-formation step were examined. Accordingly, the formation of the major stereoisomeric products is most plausible by one of the bifunctional pathways

that involve electrophile activation by the protonated amine group of the catalyst. However, some of the minor product isomers are also accessible through alternative reaction routes. Structural analysis of transition states points to the structural invariance of certain fragments of the transition state, such as the protonated catalyst and the anionic fragment of approaching reactants. Our topological analysis provides deeper insight and a more general understanding of bifunctional noncovalent organocatalysis.

Introduction

Bifunctional acid-base catalysis is a fundamental and enduring concept that is invoked to increase reaction rates of organic reactions and mimic, or explain, enzymatic catalysis.^[1] Although its noncovalent organocatalytic version has been around for decades,^[2] the discovery of the chiral bifunctional 1,2 tertiary amino-thiourea catalyst by Takemoto and co-workers^[3] revitalized the field. In their catalytic system, the double hydrogen-bond donor thiourea was considered to position and activate the electrophiles, while parallel activation of nucleophiles was assumed to occur by the neighboring tertiary amine. This type of catalyst has proved to be a highly efficient and versatile promoter for a wide range of synthetically important 1,2 and 1,4 nucleophile–electrophile additions.^[4,5] In addition to stereoselective methodological developments, there has been a surge of interest in bifunctional organocatalyst design, and this

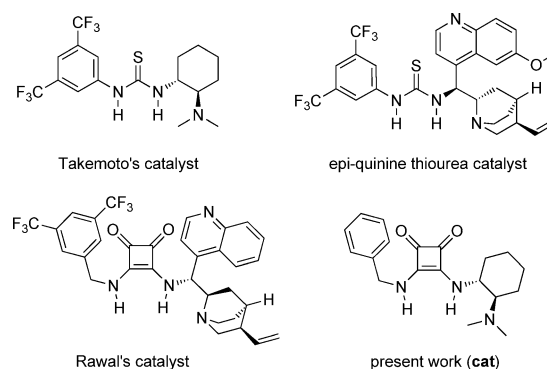


Figure 1. Bifunctional thiourea- and squaramide-based organocatalysts.

heightened activity has resulted in the evolution of some prominent catalyst variants, such as cinchona- or squaramide-based bifunctional catalysts (Figure 1).^[6,7]

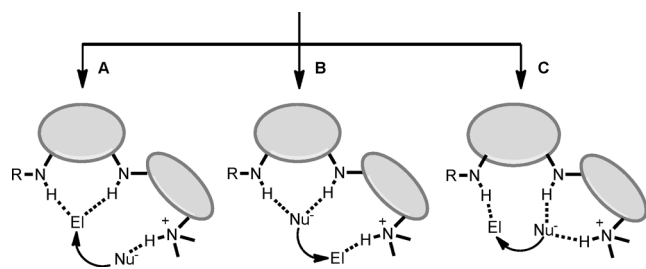
Despite a steady growth in the number and apparent impact of noncovalent bifunctional organocatalysis in the last decade, the mechanism of these processes is still far from being well understood. Although kinetic experimental studies in thiourea-amine catalysis are consistent with the dual activation mechanism, computational investigations of the rate-determining transition states indicated that the bifunctional mechanism is a blanket term covering at least three closely related mechanisms (Scheme 1).

Path A (Scheme 1), a mechanism postulated by Takemoto, involves the dual activation of the electrophile (EI) and nucleophile (Nu) by the double hydrogen-bond donor thiourea and the tertiary amine, respectively.^[8] Subsequent experimental

[a] B. Kótai, G. Kardos, Dr. A. Hamza, Dr. I. Pápai, Dr. T. Soós
Institute of Organic Chemistry
Research Centre for Natural Sciences
of the Hungarian Academy of Sciences
Pusztaszeri út 59-67
H-1025 Budapest (Hungary)
Fax: (+36) 1-438-1145
E-mail: papai.imre@ttk.mta.hu
soos.tibor@ttk.mta.hu

[b] Dr. V. Farkas
MTA-ELTE Protein Modelling Research Group
Pázmány Péter sétány 1A
H-1117 Budapest (Hungary)

Supporting information for this article is available on the WWW under <http://dx.doi.org/10.1002/chem.201304553>.



Scheme 1. Transition-state variants of the bifunctional mechanisms.

and theoretical work provided evidence that reactions promoted by bifunctional thiourea catalysts could proceed through this mechanism.^[9] The generality of this heuristic model was challenged by our theoretical studies, which suggested an alternative scenario for the rate-determining step.^[10] In this pathway (Scheme 1, Path B), the relative role of the catalytically active sites in substrate binding and activation is different. The thiourea, as an efficient anion receptor, binds the deprotonated nucleophile, while the protonated amine activates and positions the electrophile. The possibility of bifunctional catalysis through mechanism B was supported by additional theoretical and experimental results.^[11] Finally, Wang and co-workers recently suggested a variant of the bifunctional mechanism in which the distal acidic NH group of thiourea, and not the protonated amine, activates and positions the electrophile.^[12] In Path C, the deprotonated nucleophile is involved in double hydrogen bond interactions with the protonated amine and the available thiourea N–H bond. This novel mechanistic proposal was corroborated by DFT calculations on the vinylogous Michael addition of α,β -unsaturated butyrolactam to chalcone.^[12]

At first sight, the above mechanistic diversity in the rate-determining step might seem irrelevant in terms of the outcome of the organocatalytic process; however, an in-depth understanding of these elementary steps is essential for the rational design of improved catalyst systems. Furthermore, the implicit conclusion drawn from the mechanistic studies is that the structural and electronic factors of the reacting substrates determine which bifunctional pathway is followed. This, somewhat perplexing, “substrate mechanistic control” perception also raises the question of whether the preference of a given mechanistic scenario can be altered by changing the fundamental structural features of the catalysts, for instance, the distance between the catalytically essential H-bond donor units.

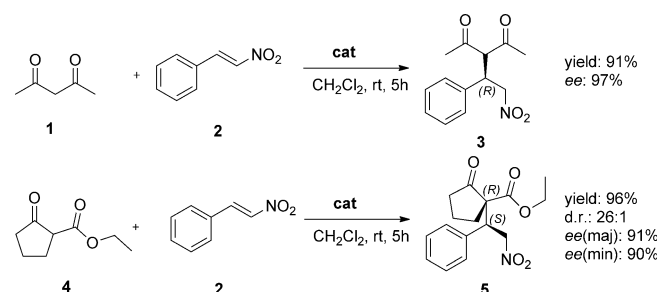
To gain more insight into these intriguing mechanistic issues, we initiated a joint experimental–theoretical study of a bifunctional squaramide-amine-catalyzed Michael addition reaction. This particular choice of catalyst seemed interesting not only because, to the best of our knowledge, no mechanistic investigations have previously been reported for squaramide-assisted bifunctional organocatalytic reactions,^[13] but also because Wang et al. prognosticated that squaramide-based bifunctional catalysis may preferentially follow Path C due to the longer distance between the N–H protons in squaramide.^[12]

Results and Discussion

Experimental background

To investigate the underlying principles of the bifunctional squaramide-amine-catalyzed Michael reactions and compare them with those of thiourea catalysis, we chose the reaction between 1,3-dioxo nucleophiles and nitrostyrene. This is one of the benchmark reactions in bifunctional thiourea- and squaramide-based organocatalysis, and affords Michael adducts with high levels of enantio- and diastereoselectivity.

As a first step, we synthesized a bifunctional diamino-cyclohexane-based squaramide catalyst (**cat**). The molecular size of this catalyst allowed computational analysis at a reasonably high level of theory. The synthesis of the catalyst was accomplished by following a reported synthetic sequence from simple and available building blocks, such as squaric acid diethyl ester and *trans*-1,2-diaminocyclohexane.^[7] In the model reaction with acetylacetone **1** and nitrostyrene **2** (Scheme 2),



Scheme 2. Enantio- and diastereoselective Michael addition to nitrostyrene.

this catalyst showed very similar catalytic performance to those of previously reported catalysts. Both the yield and the enantioinduction capacity of the catalyst **cat** were similar to those of the related catalysts previously reported.^[6a,7,14]

The possibility of an additional enantiodifferentiation capacity of **cat** was then probed by using ethyl 2-oxo-cyclopentane-carboxylate (**4**) as a prochiral nucleophile. It was found that, in addition to high levels of enantioselectivity, high level of diastereoselectivity could also be achieved, affording the product with a stereoarray including a quaternary all-carbon stereocenter (91% ee, 26:1 d.r.). The absolute and relative stereochemistry of adduct **5** was determined by vibrational circular dichroism (VCD) spectroscopic measurements.^[15] The enormous impact of the bifunctional catalyst on diastereoselectivity could be estimated by comparing the outcomes with those of the triethylamine (TEA) promoted reaction. Thus, the bifunctional squaramide **cat** was able to shift the diastereomeric ratio from 2:3 (TEA) to 26:1.

Encouraged by the result that the catalyst **cat** behaved similar to previous squaramide catalysts in the above Michael additions, we conducted density functional theory (DFT) calculations to distinguish between potential pathways A–C operating in the rate-determining step.

Conformational analysis of the catalyst

We first explored computationally the conformational space of the chiral squaramide **cat**. In these calculations, potential energy scans were performed along dihedral angles describing the relative orientation of different units of the catalyst. Structures corresponding to the located energy minima were then fully optimized, and the relative stabilities were estimated by using the protocol described in the Computational Approach section. The most stable structures that emerged from this analysis are depicted in Figure 2.

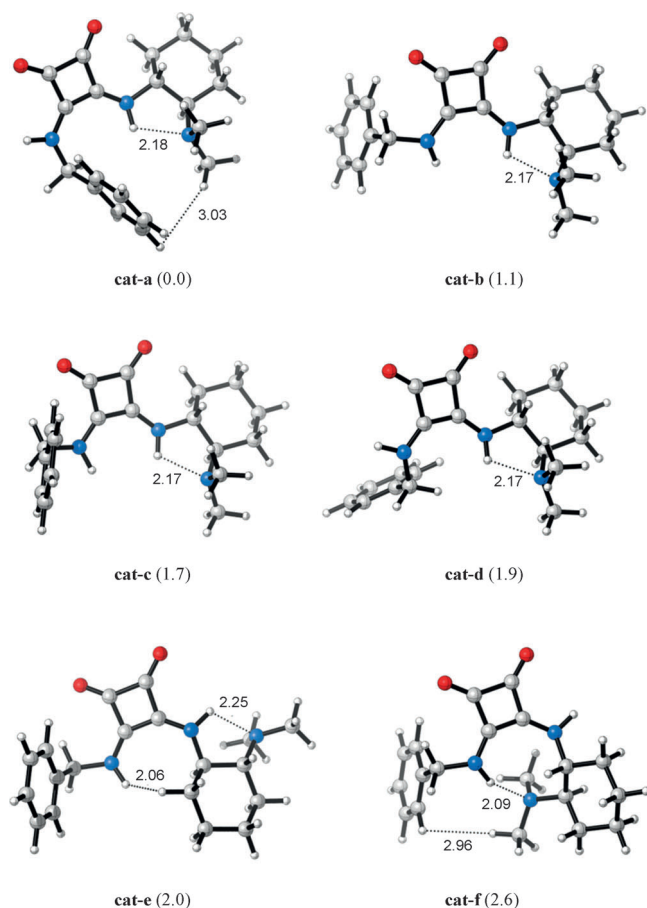


Figure 2. The most-stable conformers of catalyst **cat**. Relative free energies (in kcal mol⁻¹) are shown in parenthesis. Selected interatomic distances are given in Å.

The energetically lowest lying catalyst conformer (**cat-a**) features both an intramolecular H-bond formed between the tertiary amine and the neighboring NH group and a close contact between the benzyl and dimethylamino groups. This latter interaction seems to provide appreciable stabilization to this structure because conformer **cat-d**, which differs only in the position of the benzyl group, is predicted to be 1.9 kcal mol⁻¹ higher in free energy. Conformers **cat-b** and **cat-c** represent the active forms of the catalyst with the two N-H functionalities aligned parallel and pointing towards the amine group, forming a chiral catalytic pocket. Of the two structures, **cat-b** is

found to be slightly more favored, lying only 1.1 kcal mol⁻¹ above **cat-a**. Additional low-lying catalyst conformers with internal H-bonds and other types of weak noncovalent interactions were identified computationally (**cat-e** and **cat-f**), but they were not considered relevant to the bifunctional mechanism assumed for the present reactions.^[16]

These results suggest that the calculated conformational distribution of catalyst **cat** is similar to that found previously for the Takemoto catalyst^[10] in that the conformer that is consistent with the dual substrate activation mechanism is an energetically low-lying structure that is populated in the solution phase.

Michael addition of acetylacetone to *trans*- β -nitrostyrene

In the next stage of our study, the elementary steps of the catalytic Michael addition of acetylacetone (**1**) to *trans*- β -nitrostyrene (**2**) were analyzed, focusing on possible mechanistic pathways regarding the C–C bond formation and also on the origin of the enantioselectivity.

Calculations carried out for binary catalyst–substrate systems indicate that both reactants can form double H-bonds with the squaramide unit (see Figure 3). These binding modes are

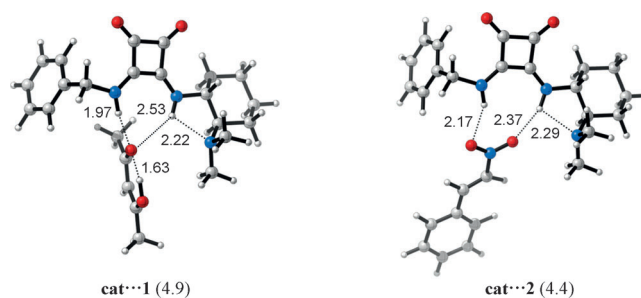


Figure 3. Double H-bonded catalyst–substrate adducts. Gibbs free energies relative to the corresponding dissociation limits (**cat+1** and **cat+2**) are shown in parenthesis (in kcal mol⁻¹).

slightly asymmetric, and both **cat...1** and **cat...2** complexes are predicted to be thermodynamically unfavored ($\Delta G > 0$). Interestingly, the enolic form of **1** displays another coordination mode, with **cat** showing a single N–H...O type hydrogen bond with the squaramide and also one O–H...N type bond (see **cat...1'** in Figure 4). This structure is slightly more favored and it can be regarded as the reactant state for the protonation of the catalyst. The proton shift occurring via **TS_{prot}** is facile and leads to an ion-pair intermediate (**catH⁺...1⁻**) lying only 1.3 kcal mol⁻¹ above the reactant level (**cat+1**). This species is stabilized through multiple H-bonds involving one NH group from the protonated amine and another from the squaramide. The H-bonded network can be expanded through internal rearrangement to structure **catH⁺...1⁻**, however, this ion-pair conformer is 4 kcal mol⁻¹ less stable than **catH⁺...1⁻**.

Three reaction pathways, corresponding to models A, B and C, have been examined for the C–C bond-formation process between the activated nucleophile **1** and electrophile **2**. Transi-

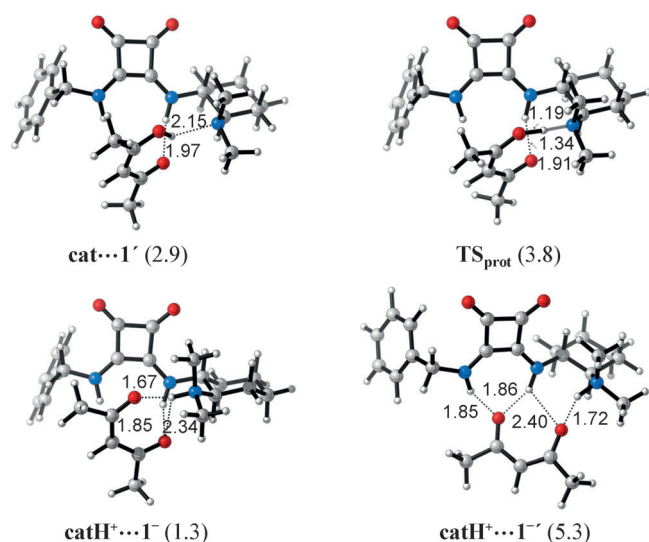


Figure 4. Deprotonation of the nucleophilic acetylacetone (**1**) substrate. Gibbs free energies relative to the **cat+1** are shown in parenthesis (in kcal mol⁻¹).

tion states for pathways A and B could be easily located with our standard computational protocol, however, all attempts to identify C-type transition states failed. Our detailed analysis indicates that the transition state of C–C bond formation is not compatible with the H-bonding pattern defined by model C.^[15]

For reaction pathway A, the most stable transition state (**TS-A-R₁** in Figure 5) is consistent with the formation of the (*R*) stereoisomer of adduct **3**, which is the major product observed experimentally. In this structure, the enolate ion is attached to the protonated amine through N–H...O and C–H...O type hydrogen bonds, whereas nitrostyrene forms double H-bond with

the squaramide NH units. The activation barrier represented by **TS-A-R₁** is 19.3 kcal mol⁻¹ with respect to the separated reactants (**cat+1+2**). A slightly less stable transition state with similar binding features, but different relative positioning of the H-bond donor and acceptor sites was located on this pathway (see **TS-A-R₂** in Figure 5), pointing to a certain degree of structural flexibility of the stabilizing H-bonding network. The enantiomeric adduct (*S*)-**3** forms via **TS-A-S₁** and the computed activation barrier is 20.8 kcal mol⁻¹. Again, an additional transition state (**TS-A-S₂**) with a slightly higher barrier was found in our calculations. It should be noted that in these latter two structures, only one of the –NO₂ oxygen atoms engaged in H-bonding with squaramide, thus the ideal double H-bonding pattern is not established.

On reaction pathway B, the most favored transition state (**TS-B-R₁** in Figure 6) provides a barrier of 15.5 kcal mol⁻¹ for C–C bond formation, which is significantly lower than that found for Path A. This structure is characterized by a multiple H-bonding pattern between the enolate and the squaramide, wherein one of the carbonyl groups is bound to both NH units and the second is involved in a single N–H...O bond shifted towards the benzyl group of the catalyst. The nitro group of the electrophile is bound to the protonated amine, which stabilizes the negative charge developing on this unit upon C–C bond formation. Interestingly, an additional transition state having a slightly different structure (the enolate shifted in the opposite direction to the squaramide, that is, towards the cyclohexyl group) could also be identified (**TS-B-R₂**), which was only 1.5 kcal mol⁻¹ less stable than the former structure. In contrast to bifunctional thioureas,^[10] bifunctional squaramides thus provide multiple reaction channels in this reaction even for a given type of mechanistic pathway.

Along Path B, the computational analysis located two analogous transition states leading to the minor enantiomeric product. Those processes are predicted to be significantly less favored in free energy (see **TS-B-S₁** and **TS-B-S₂** in Figure 6). It is worth pointing out that the barrier represented by **TS-B-S₁** is only 0.7 kcal mol⁻¹ lower than that arising from **TS-A-S₁** on the other route, suggesting a scenario in which a clear preference for model B can be established for the formation of the major product, however, the minor product species can be produced through both pathways.

The relative free energies of the entire set of transition states are collected in Table 1 along with their contributions to the formation of (*R*) and (*S*) product isomers. These results point to

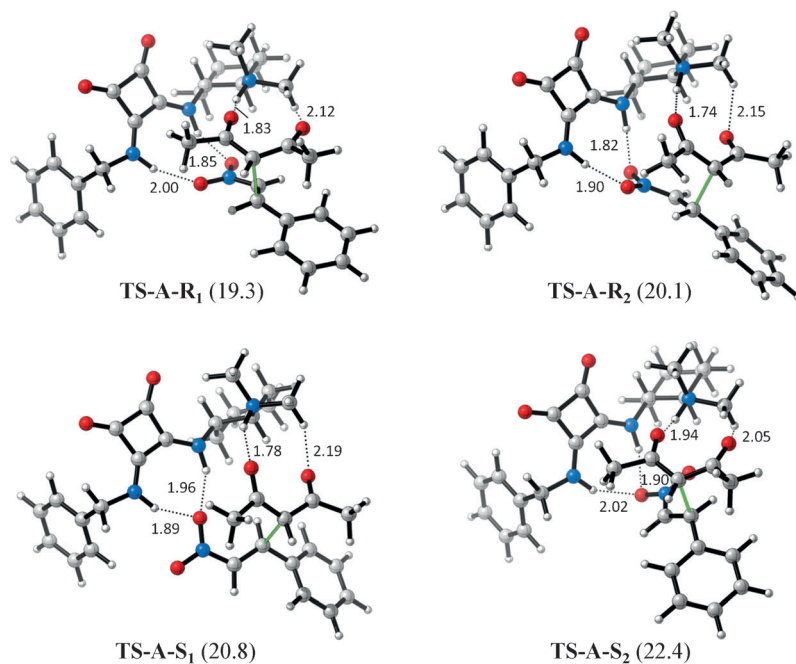


Figure 5. Transition states identified on Path A for the reaction of **1** and **2**. Predicted activation barriers (in kcal mol⁻¹; computed as Gibbs free energies relative to **cat+1+2**) are given in parenthesis.

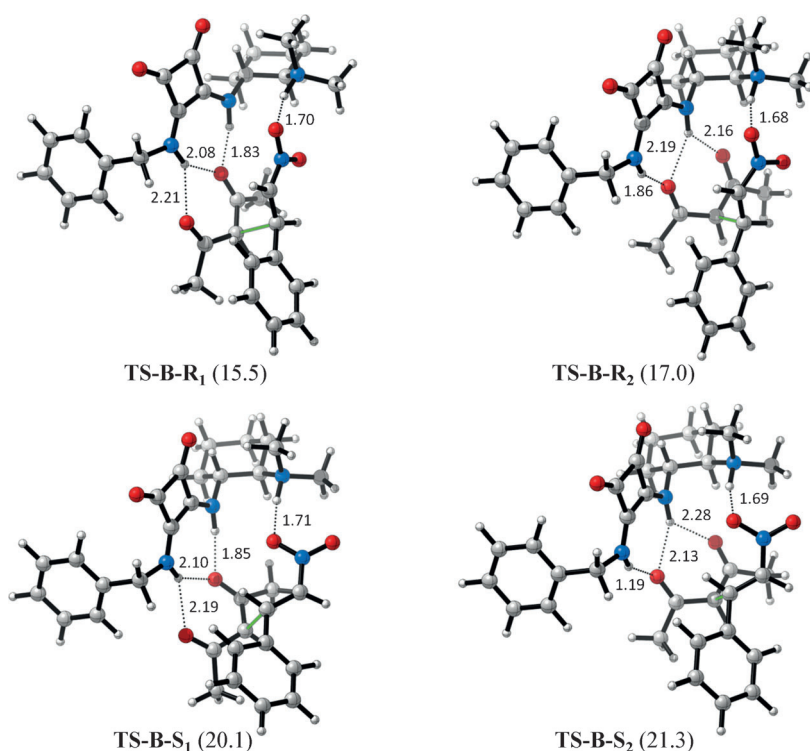


Figure 6. Transition states identified on Path B in the reaction of **1** and **2**. Predicted activation barriers (in kcal mol⁻¹; computed as Gibbs free energies relative to **cat**+**1**+**2**) are given in parenthesis.

Table 1. Relative Gibbs free energies of the located transition states and related product distribution for the reaction between 1 and 2 . ^[a]				
Path	Product	TS	ΔG [kcal mol ⁻¹]	p_i [%]
A	(R)	TS-A-R ₁	19.3	0.2
		TS-A-R ₂	20.1	0.0
	(S)	TS-A-S ₁	20.8	0.0
		TS-A-S ₂	22.4	0.0
B	(R)	TS-B-R ₁	15.5	92.6
		TS-B-R ₂	17.0	7.2
	(S)	TS-B-S ₁	20.1	0.0
		TS-B-S ₂	21.3	0.0

[a] Relative contribution of various pathways to the formation of **3** are obtained from Maxwell-Boltzmann statistics: $p_i = 100 \times \exp(-\Delta G_i/RT) / \sum_j (\exp(-\Delta G_j/RT))$.

a very high degree of enantioselectivity for the investigated reaction. However, the predicted enantiomeric ratio is much higher than that observed experimentally. This might be partially due to the inaccuracy of the present computational approach, but one cannot exclude that other unexplored reaction pathways (e.g., simple base catalysis involving solely the dimethylamino group) may operate in addition to the bifunctional mechanism.^[17]

Michael addition of ethyl-2-oxocyclopentanecarboxylate to *trans*- β -nitrostyrene

The C–C bond formation transition states were also explored for the reaction of ethyl 2-oxocyclopentanecarboxylate (**4**) with

2 (see Scheme 2). Based on our experience with the previous reaction, we considered only pathways A and B for computations. Because substrate **4** is a prochiral Michael donor, four different stereoisomeric products can be formed in this addition process, depending on the facial approach of the reactants. A schematic view of the corresponding transition states on pathways A and B is depicted in Figure 7 and Figure 8.

The conformational space of these transition states is rather complex. In addition to the structural flexibility with respect to the relative positions of the H-bond donor and acceptor sites, two puckered conformations of the five-membered ring of the enolate (**4**⁻) had to be considered in the transition-state search procedure. Consequently, we identified four different tran-

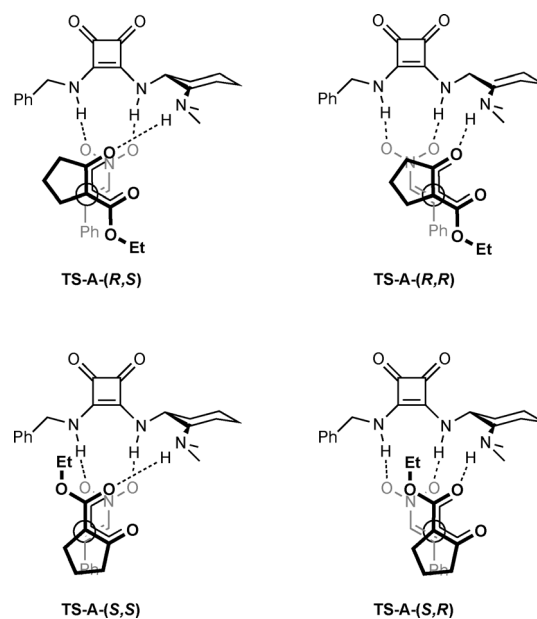


Figure 7. Schematic view of transition states leading to various product isomers along Path A in the reaction of **4** and **2**.

sition structures for each facial approach. These structures are reported in the Supporting Information. Herein, we analyze only the most stable forms of the transition states, which are depicted in Figure 9 and Figure 10; the relative free energies are collected in Table 2.

The H-bonding patterns of the located transition states resemble those of the previous reaction and reflect the structural

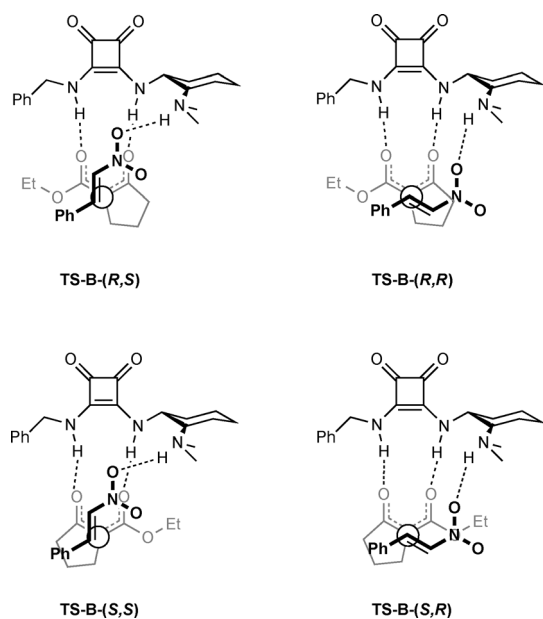


Figure 8. Schematic view of transition states leading to various product isomers along Path B in the reaction of **4** and **2**.

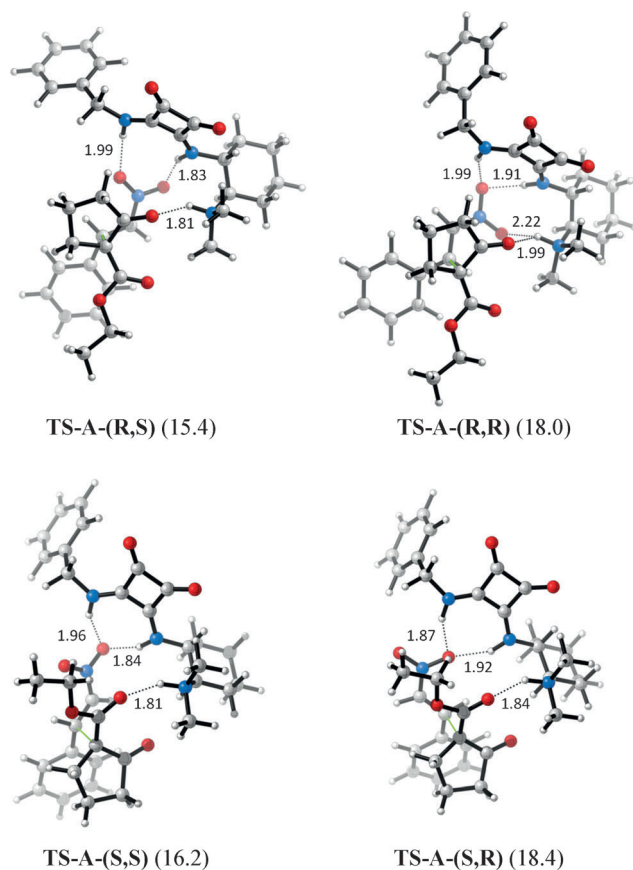


Figure 9. Most-favored transition states identified on Path A for the reaction of **4** and **2**. Predicted activation barriers (in kcal mol⁻¹; computed as Gibbs free energies relative to **cat**+**4**+**2**) are given in parenthesis.

flexibility of these systems. On Route A, the nitroolefin is bound through either one or both oxygen atoms to the squaramide, whereas on Route B, the enolate is attached to this unit

Table 2. Relative Gibbs free energies of the located transition states and related product distribution for the reaction between 4 and 2 . ^[a]				
Path	Product	TS	ΔG [(kcal mol ⁻¹)]	p_i [%]
A	(<i>R,R</i>)	TS-A-(<i>R,R</i>)	18.0	0.0
	(<i>R,S</i>)	TS-A-(<i>R,S</i>)	15.4	0.3
	(<i>S,R</i>)	TS-A-(<i>S,R</i>)	18.4	0.0
	(<i>S,S</i>)	TS-A-(<i>S,S</i>)	16.2	0.1
B	(<i>R,R</i>)	TS-B-(<i>R,R</i>)	17.2	0.0
	(<i>R,S</i>)	TS-B-(<i>R,S</i>)	12.0	92.0
	(<i>S,R</i>)	TS-B-(<i>S,R</i>)	19.1	0.0
	(<i>S,S</i>)	TS-B-(<i>S,S</i>)	15.0	0.5

[a] Relative contribution of various pathways to the formation of product isomers are obtained from Maxwell-Boltzmann statistics: $p_i = 100 \times \exp(-\Delta G_i/RT) / \sum_j \exp(-\Delta G_j/RT)$ using the entire set of transition states (reported in Table S1 of the Supporting Information).

by three N-H...O bonds and it is shifted from the symmetrical arrangement to either the benzyl or cyclohexyl moieties of the catalyst molecule.

Calculations predict the preferential formation of the (*R,S*) product for route A, which is in line with experimental findings (the barriers represented by TS-A-(*R,S*) and TS-A-(*S,R*) differ by 3.0 kcal mol⁻¹). However, the observed high diastereomeric ratio (26:1) cannot be rationalized by this model, because the (*S,S*) diastereomeric product is calculated to be formed through a relatively small barrier [TS-A-(*S,S*) is only 0.8 kcal mol⁻¹ less stable than TS-A-(*R,S*)]. On the other hand, model B predicts high enantio- and diastereoselectivity for this reaction, because the four transition states are significantly separated in free energy. For the major (*R,S*) product, the barrier is found to be much lower on Route B (by 3.4 kcal mol⁻¹), whereas for the other stereoisomers the computed barriers are quite similar on the two reaction pathways. Consequently, these stereoisomers are accessible through both reaction channels A and B. As a matter of fact, the (*S,R*) enantiomeric product is predicted to be formed preferentially through Route A.

Additional mechanistic insights from the structural analysis

The work described above reinforces the conclusion that the underlying mechanistic principles in bifunctional squaramide and bifunctional thiourea catalysis are the same. However, there are some additional features for squaramide catalysis that can be related to the elongated distance between the N-H bonds of the squaramide. It was found that catalyst **cat** provides multiple transition states even within a given reaction pathway. These energetically close-lying subvariant transition structures differ slightly in the geometries and the pattern in the hydrogen bonds, and inevitably increase the complexity of the mechanism. Furthermore, the overall mechanistic picture becomes even more complex by considering that some of the stereoisomeric products seem to be formed in parallel through two distinct pathways. Although, these findings can be interpreted as providing new insight, such mechanistic complexity results in a much less general understanding and definitely limits the potential of knowledge-based approaches in future catalyst development.

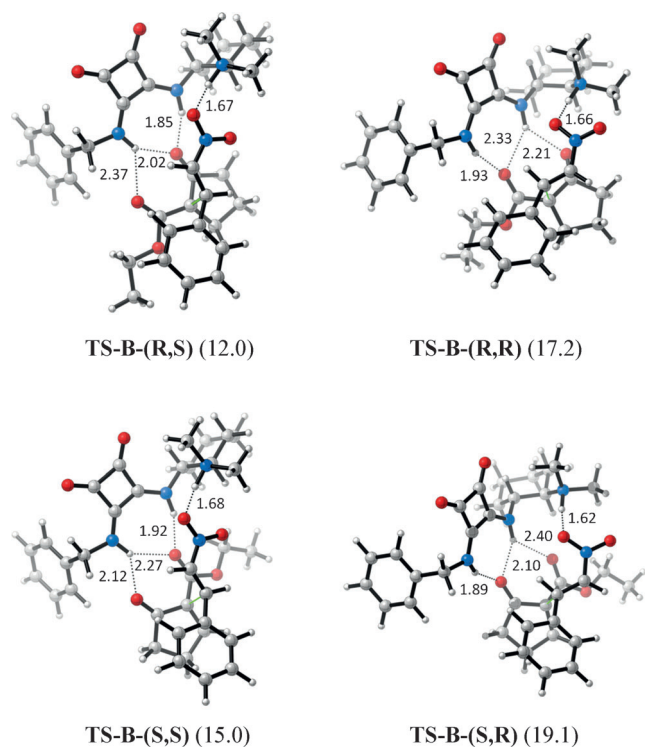


Figure 10. Most-favored transition states identified on Path B for the reaction of **4** and **2**. Predicted activation barriers (in kcal mol⁻¹; computed as Gibbs free energies relative to **cat**+**4**+**2**) are given in parenthesis.

To develop a more general view on the investigated mechanism, we carried out a detailed topological analysis of some of the transition states identified for the reaction of **1** and **2**. In this analysis, we superimposed various transition states and examined the structural variation of two fragments, namely the protonated catalyst and the remaining anionic adduct-like species.

We first generated an overlay of the two most stable transition states obtained for routes A and B (**TS-A-R₁** and **TS-B-R₁**). In Figure 11a, the protonated catalyst fragments of the two transition states are superimposed at the cyclohexyl groups. Surprisingly, the two structures appear to be rather similar; only a slight variation in the orientation of the squaramide unit can be observed. The overlay of the anionic fragments reveal almost identical geometries (see Figure 11b), illustrating that

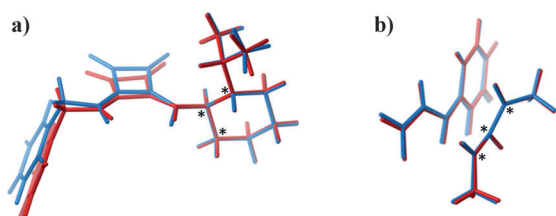


Figure 11. Overlays of transition states **TS-A-R₁** (blue) and **TS-B-R₁** (red). a) The protonated catalyst superimposed via the cyclohexyl group, and b) anionic adduct fragments (the superimposed atoms are indicated by asterisks). The complementary fragments are omitted for clarity.

the mutual approach of reactants is also structurally well-defined regardless of which pathway they follow.

We then compared the structures of transition states **TS-B-R₁** and **TS-B-S₁**, which correspond to the most favored transition states leading to the formation of enantiomeric *R* or *S* products, respectively. Similarly to the previous case, the position and the orientation of the NH groups of the protonated catalyst match remarkably well in the two structures (see Figure 12). Surprisingly, the H-bonding patterns show close resemblance in the two transition states. Of the four oxygen

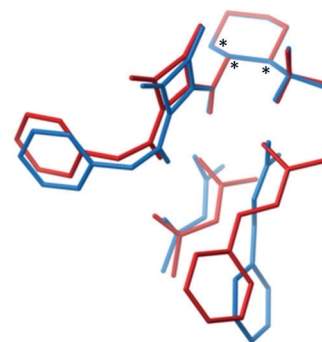


Figure 12. Overlays of transition states **TS-B-R₁** (blue) and **TS-B-S₁** (red) superimposed via the cyclohexyl group of the protonated catalyst (the superimposed atoms are indicated by asterisks). H atoms are omitted for clarity (except those involved in H-bonding).

atoms of the reacting species, three are involved in hydrogen bonding and their positions relative to the chiral H-bond donor environment are structurally invariant.

Based on the above fragment analysis, a more general mechanistic picture begins to emerge. The results suggests that the protonated catalyst formed upon the activation of acetylacetone acts as a chiral oxyanion hole in this reaction and stabilizes the anionic transition state of the approaching reactants. Although the positions of the H-bond donor sites of the oxyanion hole and the acceptor sites of the anionic species are well-defined, several H-bonding patterns are available, giving rise to different reaction pathways for the C–C bond-formation process and even to similar parallel reaction channels. The feasibility of these pathways and the stereoisomeric preference are determined by the strength of the H-bonding network formed between the two structurally invariant fragments.

Conclusion

We have conducted combined experimental and theoretical investigations on Michael addition reactions promoted by the bi-functional squaramide tertiary amine organocatalyst **cat**. Based on the presented results, the following conclusions can be drawn. The mechanism of the present squaramide-catalyzed reaction is analogous to that reported for thiourea catalysis in terms of the basic elementary steps and the relative importance of previously proposed reactivity models. We found that reaction pathway B, corresponding to electrophile activation

via the protonated amine unit of the catalyst, is the most plausible mechanism, which accounts reasonably well for the observed stereoselectivity. An interesting new feature of the squaramide-catalyzed reaction is that some of the reaction channels described as pathway A also become accessible, implying that the application of a single reactivity model might not always be sufficient to rationalize the stereoselectivity outcome of Michael addition reactions. The previously envisioned Path C could not be identified as a viable mechanism for the present reaction.

An additional feature of squaramide catalysis is the existence of energetically close-lying multiple transition states within the same pathway, differing only in the relative positions of H-bond acceptor sites with respect to the squaramide NH bonds. This is likely related to the increased H...H distance in squaramide (2.7 vs. 2.1 Å in thiourea), which offers alternative binding modes for the acceptor sites.

The overlay analysis of transition-state fragments revealed that the protonated catalyst creates a geometrically invariant chiral oxyanion hole. The topology of the acceptor oxygen atoms of the anionic transition state fragment of reacting species is also well-defined, therefore, the competing mechanistic pathways can be unified under the concept of transition-state tethering to the chiral oxyanion hole. This theoretical view simplifies and explains the mechanism, suggesting that it is the best fitting to the structurally rigid chiral oxyanion hole that determines not only which pathway operates, but also which enantiomer will be delivered in the catalytic cycle.

Due to the loose nature of hydrogen-bonding interactions, the optimal H-bonding pattern cannot be easily predicted even when the structures of the protonated catalyst and the anionic fragment are available. However, the present findings may help in the development of more efficient computational tools for transition-state analysis, which may aid the design of new catalysts. The development of force-field-based transition-state screening methods is in progress in our laboratory.

Experimental Section

General synthetic procedure

Catalyst **cat** (5 mol%, 0.05 mmol) was added to a mixture of nitrostyrene **2** (149.2 mg, 1.0 mmol) and the appropriate nucleophile (2.0 mmol) in dichloromethane (2 mL) and the mixture was stirred for 5 h at RT until the reaction was complete (followed by TLC analysis). The reaction mixture was then concentrated in vacuo and the crude product was subjected to column chromatography (hexane/ethyl acetate, 5:1 to 1:1).

Computational approach

The geometries of the stationary points were optimized by using density functional theory (DFT) with the B3LYP functional^[18] and the 6-31G(d) basis set. To provide accurate energetics, additional single-point energy calculations were carried out for each structure at the M06-2X/6-311++G(d,p) level of theory.^[19] In these calculations, the ultrafine integration grid was employed to ensure accuracy of numerical integration. The M06-2X functional was previously shown to perform reasonably for Michael addition reactions.^[20]

The application of the B3LYP functional for geometry optimizations (and subsequent single-point calculations at higher level) was also justified in previous work.^[21]

The nature of the stationary points was characterized by using vibrational analysis. The initial structures for transition-state calculations were determined from the potential energy surface scan calculations with respect to selected internal coordinates, which were then followed by transition-state optimizations. The harmonic frequencies were computed at the B3LYP/6-31G(d) level. These data were also utilized to estimate the zero-point energies as well as the thermal and entropic contributions to the Gibbs free energies. The thermochemical data were obtained within the ideal-gas-rigid-rotor-harmonic-oscillator approximation for $T=298.15$ K and $p=1$ atm, however, concentration correction (0.00302 a.u.) was applied to Gibbs free energies corresponding to $c=1$ mol/dm³ conditions in solvent phase. Solvent effects were also taken into account at the B3LYP/6-31G(d) level by estimating the solvation free energies (solvent=dichloromethane) by using the integral equation formalism variant of the polarizable continuum model (IEFPCM).^[22] The atomic radii and nonelectrostatic terms in the IEFPCM calculations were those introduced recently by Truhlar and co-workers (SMD solvation model).^[23]

The energy values reported in the paper correspond to solution-phase Gibbs free energies, which are based on M06-2X/6-311++G(d,p) electronic energies, and all additional terms were obtained at the B3LYP/6-31G(d) level. All DFT calculations were carried out with the Gaussian 09 software.^[24]

Acknowledgements

We are grateful for the financial support of the Hungarian Scientific Research Fund (OTKA, grants K-69086 and K-81927) and the Lendület Program E-13/11/2010.

Keywords: density functional calculations · Michael addition · organocatalysis · reaction mechanisms · reaction intermediates

- [1] a) T. M. Lowry, I. J. Falkner, *J. Chem. Soc., Trans.* **1925**, 127, 2883; b) T. M. Lowry, I. J. Falkner, *J. Chem. Soc.* **1927**, 2554; c) H. D. Paull, C. J. Abraham, M. T. Scerba, E. Alden-Danforth, T. Lectka, *Acc. Chem. Res.* **2008**, 41, 655; d) T. Setoyama, *Catal. Today* **2006**, 116, 250; e) M. Shibasaki, N. Yoshikawa, *Chem. Rev.* **2002**, 102, 2187; f) *Catalysis by Acid and Bases* (Eds.: K. Tanabe, B. Imelik, C. Naccache, G. Coudurier, Y. Ben Taarit, J. C. Vedrine), Elsevier, Amsterdam, **1985**; g) H. Steinhagen, G. Helmchen, *Angew. Chem.* **1996**, 108, 2489; *Angew. Chem. Int. Ed. Engl.* **1996**, 35, 2339; h) J. D. Wuest, *Acc. Chem. Res.* **1999**, 32, 81; i) J.-M. Ma, D. Cahard, *Angew. Chem.* **2004**, 116, 4666; *Angew. Chem. Int. Ed.* **2004**, 43, 4566.
- [2] a) C. G. Swain, J. F. Brown, *J. Am. Chem. Soc.* **1952**, 74, 2534; b) W. P. Jencks, *Chem. Rev.* **1972**, 72, 705; c) H. Hiemstra, H. Wynberg, *J. Am. Chem. Soc.* **1981**, 103, 417.
- [3] T. Okino, Y. Hoashi, Y. Takemoto, *J. Am. Chem. Soc.* **2003**, 125, 12672.
- [4] For recent books on organocatalysis, see: a) *Comprehensive Enantioselective Organocatalysis: Catalysts, Reactions, and Applications* (Ed.: P. I. Dalko), Wiley-VCH, Weinheim, **2013**; b) *Science of Synthesis: Asymmetric Organocatalysis Volume 2* (Ed.: K. Maruoka), Thieme, Stuttgart, **2012**.
- [5] For recent reviews, see: a) J. Alemán, A. Parra, H. Jiang, K. A. Jørgensen, *Chem. Eur. J.* **2011**, 17, 6890; b) W.-Y. Siau, J. Wang, *Catal. Sci. Technol.* **2011**, 1, 1298; c) S. J. Connon, *Chem. Commun.* **2008**, 2499.
- [6] For seminal works on catalyst development, see: a) J. P. Malerich, K. Hagihara, V. H. Rawal, *J. Am. Chem. Soc.* **2008**, 130, 14416; b) B. Vakulya, S. Varga, A. Csámpai, T. Soós, *Org. Lett.* **2005**, 7, 1967; c) S. H. McCooney, S. J. Connon, *Angew. Chem.* **2005**, 117, 6525; *Angew. Chem. Int. Ed.* **2005**, 44, 6367; d) J. Ye, D. J. Dixon, P. S. Hynes, *Chem. Commun.* **2005**,

- 4481; e) B.-J. Li, L. Jiang, M. Liu, Y.-C. Chen, L.-S. Ding, Y. Wu, *Synlett* **2005**, 603; f) see ref. [3].
- [7] For recent selected examples using bifunctional squaramides, see: a) K. S. Yang, A. E. Nibbs, Y. E. Turkmen, V. H. Rawal, *J. Am. Chem. Soc.* **2013**, *135*, 16050; b) Y. Fukata, K. Asano, S. Matsubara, *J. Am. Chem. Soc.* **2013**, *135*, 12160; c) Y. Liu, Y. Wang, H. Song, Z. Zhou, *Adv. Synth. Catal.* **2013**, *355*, 2544; d) Q. Guo, J. C.-G. Zhao, *Org. Lett.* **2013**, *15*, 508; e) X. Fang, J. Li, C.-J. Wang, *Org. Lett.* **2013**, *15*, 3448; f) X. Fang, Q.-H. Li, H.-Y. Tao, C.-J. Wang, *Adv. Synth. Catal.* **2013**, *355*, 327; g) M.-X. Zhao, H.-L. Bi, H. Zhou, H. Yang, M. Shi, *J. Org. Chem.* **2013**, *78*, 9377; h) H. Wang, Y. Wang, H. Song, Z. Zhou, C. Tang, *Eur. J. Org. Chem.* **2013**, 4844; i) W. Yang, Y. Yang, D.-M. Du, *Org. Lett.* **2013**, *15*, 1190; j) C. C. J. Loh, D. Hack, D. Enders, *Chem. Commun.* **2013**, *49*, 10230; k) C. Jarava-Barrera, F. Esteban, C. Navarro-Ranninger, A. Parra, J. Alemán, *Chem. Commun.* **2013**, *49*, 2001; l) G. Kardos, T. Soós, *Eur. J. Org. Chem.* **2013**, 4490.
- [8] T. Okino, Y. Hoashi, Y. Takemoto, *J. Am. Chem. Soc.* **2005**, *127*, 119.
- [9] a) S. J. Zuend, E. N. Jacobsen, *J. Am. Chem. Soc.* **2007**, *129*, 15872; b) P. Hammar, T. Marcelli, H. Hiemstra, F. Himo, *Adv. Synth. Catal.* **2007**, *349*, 2537; c) S. J. Zuend, E. N. Jacobsen, *J. Am. Chem. Soc.* **2009**, *131*, 15358.
- [10] A. Hamza, G. Schubert, T. Soós, I. Pápai, *J. Am. Chem. Soc.* **2006**, *128*, 13151.
- [11] a) D. Almasi, D. A. Alonso, E. Gómez-Bengoa, C. Nájera, *J. Org. Chem.* **2009**, *74*, 6163; b) B. Tan, Y. Lu, X. Zeng, P. J. Chua, G. Zhong, *Org. Lett.* **2010**, *12*, 2682; c) X. Han, R. Lee, T. Chen, J. Luo, Y. Lu, K. W. Huang, *Sci. Rep.* **2013**, *3*, 2557; d) T. Azuma, Y. Kobayashi, K. Sakata, T. Sasamori, N. Tokitoh, Y. Takemoto, *J. Org. Chem.* **2014**, *79*, 1805.
- [12] J.-L. Zhu, Y. Zhang, C. Liu, A.-M. Zheng, W. Wang, *J. Org. Chem.* **2012**, *77*, 9813.
- [13] For recent theoretical work on bifunctional squaramide-enamine catalysis, see: T. Lu, S. E. Wheeler, *Chem. Eur. J.* **2013**, *19*, 15141.
- [14] a) H. Y. Bae, S. Some, J. S. Oh, Y. S. Lee, C. E. Song, *Chem. Commun.* **2011**, *47*, 9621; b) C. Min, X. Han, Z. Liao, X. Wu, H.-B. Zhou, C. Dong, *Adv. Synth. Catal.* **2011**, *353*, 2715.
- [15] For details see the Supporting Information.
- [16] For a related NMR study, see: G. Tárkányi, P. Király, T. Soós, S. Varga, *Chem. Eur. J.* **2012**, *18*, 1918.
- [17] As noted by one of the referees, transition states derived from the *E* isomer of enolate 1^- may also be competitive in this reaction. Our preliminary calculations indicate that some of these alternative pathways are indeed feasible; however, the large energy difference between the *R*- and *S*-type transition states (i.e., the overestimation of enantioselectivity) is maintained. For a related computational study highlighting the relevance of *E*-enolates in organocatalytic addition reactions, see: L. Simón, J. M. Goodman, *J. Am. Chem. Soc.* **2012**, *134*, 16869.
- [18] A. D. Becke, *J. Chem. Phys.* **1993**, *98*, 5648.
- [19] Y. Zhao, D. G. Truhlar, *Theor. Chem. Acc.* **2008**, *120*, 215.
- [20] T. A. Rokob, A. Hamza, I. Pápai, *Org. Lett.* **2007**, *9*, 4279.
- [21] L. Simón, J. M. Goodman, *Org. Biomol. Chem.* **2011**, *9*, 689.
- [22] J. Tomasi, B. Mennucci, E. Cancès, *J. Mol. Struct.* **1999**, *464*, 211.
- [23] A. V. Marenich, C. J. Cramer, D. G. Truhlar, *J. Phys. Chem. B* **2009**, *113*, 6378.
- [24] Gaussian 09, Revision A.02, M. J. Frisch, G. W. Trucks, H. B. Schlegel, G. E. Scuseria, M. A. Robb, J. R. Cheeseman, G. Scalmani, V. Barone, B. Mennucci, G. A. Petersson, H. Nakatsuji, M. Caricato, X. Li, H. P. Hratchian, A. F. Izmaylov, J. Bloino, G. Zheng, J. L. Sonnenberg, M. Hada, M. Ehara, K. Toyota, R. Fukuda, J. Hasegawa, M. Ishida, T. Nakajima, Y. Honda, O. Kitao, H. Nakai, T. Vreven, J. A. Montgomery, J. E. Peralta, F. Ogliaro, M. Bearpark, J. J. Heyd, E. Brothers, K. N. Kudin, V. N. Staroverov, R. Kobayashi, J. Normand, K. Raghavachari, A. Rendell, J. C. Burant, S. S. Iyengar, J. Tomasi, M. Cossi, N. Rega, J. M. Millam, M. Klene, J. E. Knox, J. B. Cross, V. Bakken, C. Adamo, J. Jaramillo, R. Gomperts, R. E. Stratmann, O. Yazyev, A. J. Austin, R. Cammi, C. Pomelli, J. W. Ochterski, R. L. Martin, K. Morokuma, V. G. Zakrzewski, G. A. Voth, P. Salvador, J. J. Dannenberg, S. Dapprich, A. D. Daniels, O. Farkas, J. B. Foresman, J. V. Ortiz, J. Cioslowski, D. J. Fox, Gaussian, Inc., Wallingford CT, **2009**.

Received: November 20, 2013

Published online on ■ ■ ■, 0000

FULL PAPER

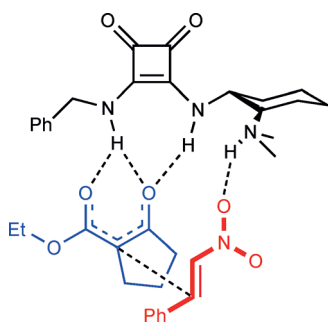
Reaction Mechanisms

B. Kótai, G. Kardos, A. Hamza, V. Farkas,
I. Pápai,* T. Soós*

■■ - ■■



On the Mechanism of Bifunctional
Squaramide-Catalyzed Organocatalytic
Michael Addition; Protonated Catalyst
as an Oxyanion Hole



Finding the path: The mechanism of bifunctional squaramide-promoted Michael addition of prochiral 1,3-dioxo nucleophiles and nitroolefin has been studied on the basis of DFT calculations. Among the investigated mechanistic scenarios, the pathway corresponding to electrophile activation via the protonated amine unit is found to be the most feasible (see figure). For some of the minor stereoisomeric products, alternative pathways are also accessible.